ACS APPLIED MATERIALS & INTERFACES

Research Article

www.acsami.org

Templated Repair of Long Bone Defects in Rats with Bioactive Spiral-Wrapped Electrospun Amphiphilic Polymer/Hydroxyapatite Scaffolds

Artem B. Kutikov,[†,‡] Jordan D. Skelly,[†] David C. Ayers,[†] and Jie Song*[,†,‡]

[†]Department of Orthopedics and Physical Rehabilitation and [‡]Department of Cell and Developmental Biology, University of Massachusetts Medical School, 55 Lake Avenue North, Worcester, Massachusetts 01655, United States

Supporting Information

ABSTRACT: Effective repair of critical-size long bone defects presents a significant clinical challenge. Electrospun scaffolds can be exploited to deliver protein therapeutics and progenitor cells, but their standalone application for long bone repair has not been explored. We have previously shown that electrospun composites of amphiphilic poly(D,L-lactic acid)-*co*-poly(ethylene glycol)-*co*-poly(D,L-lactic acid) (PELA) and hydroxyapatite (HA) guide the osteogenic differentiation of bone marrow stromal cells (MSCs), making these scaffolds uniquely suited for evaluating cell-based bone regeneration approaches. Here we examine whether the in vitro bioactivity of these electrospun scaffolds can be exploited for long bone defect repair, either through the participation of exogenous MSCs or through the activation of endogenous cells by a low dose of recombinant human bone morphogenetic protein-2 (rhBMP-2). In critical-size rat femoral segmental defects, spiral-wrapped electrospun HA−PELA with preseeded MSCs resulted in laminated endochondral ossification templated by the scaffold across the longitudinal span of the defect. Using GFP labeling, we confirmed that the exogenous MSCs adhered to HA−PELA survived at least 7 days postimplantation, suggesting direct participation of these exogenous cells in templated bone formation. When loaded with 500 ng of rhBMP-2, HA−PELA spirals led to more robust but less clearly templated bone formation than MSC-bearing scaffolds. Both treatment groups resulted in new bone bridging over the majority of the defect by 12 weeks. This study is the first demonstration of a standalone bioactive electrospun scaffold for templated bone formation in critical-size long bone defects.

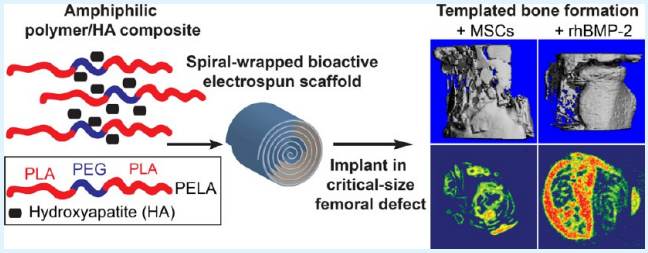

KEYWORDS: *electrospinning, amphiphilic polymer, hydroxyapatite, bone tissue engineering, bone marrow derived stromal cells, BMP (bone morphogenetic protein)*

1. INTRODUCTION

There remains a significant clinical need for better strategies to repair critical-size bone defects resulting from congenital conditions, trauma, or tumor resection. Autografting procedures are considered the gold standard, but they can lead to significant donor site morbidity and are limited by autograft supply.[1] Allografts, obtained from human donors, are alternatives to autografts but carry an inherent risk for disease transition and suffer from long-term failure rates as high as 60% over 10 years.[2] Current commercially available bone graft substitutes are typically weak and brittle gels or foams that possess poor handling characteristics (e.g., inconvenient surgical insertion and inadequate graft fixation) and limited bioactivity.[3] Adequate bone healing facilitated by these materials typically requires the delivery of high doses of exogenous growth factors such as recombinant human bone morphogenetic protein-2 (rhBMP-2). Meanwhile, commercially available bone graft substitutes are not optimized to support efficient delivery of exogenous stem/progenitor cells or guide their in vivo differentiation. The performance of bone graft substitutes can potentially be improved through tissue engineering approaches that combine biomaterials exhibiting desired physical and biological properties with safe loading doses of biological factors and/or effectively delivered skeletal progenitor cells.

Electrospinning is a widely used technique to manufacture tissue engineering scaffolds with nanofibrous morphology similar to that of native extracellular matrices.[4] Such scaffolds provide a high surface area for cell attachment and proliferation[4] and when properly engineered can also guide stem cell differentiation.[5−7] As growth factor delivery vehicles, the high surface area of electrospun scaffolds is desired for protein adsorption and improved sustained release.[8] For bone tissue engineering, electrospun composites combining degradable polymers with osteoconductive minerals such as hydroxyapatite (HA) have been shown to promote osteogenic differentiation of bone progenitor cells, especially when the HA is well integrated with the polymer matrix.[7,9−11] However,

Received: December 19, 2014
Accepted: February 6, 2015
Published: February 19, 2015

DOI: 10.1021/am508984y
ACS Appl. Mater. Interfaces 2015, 7, 4890−4901

Scheme 1. Schematic of the Spiral Wrapping of HA−PELA Scaffolds with or without Preseeded Cells or Absorbed rhBMP-2 for Implantation Into a 5 mm Rat Femoral Segmental Defect Stabilized by a PEEK Fixation Plate

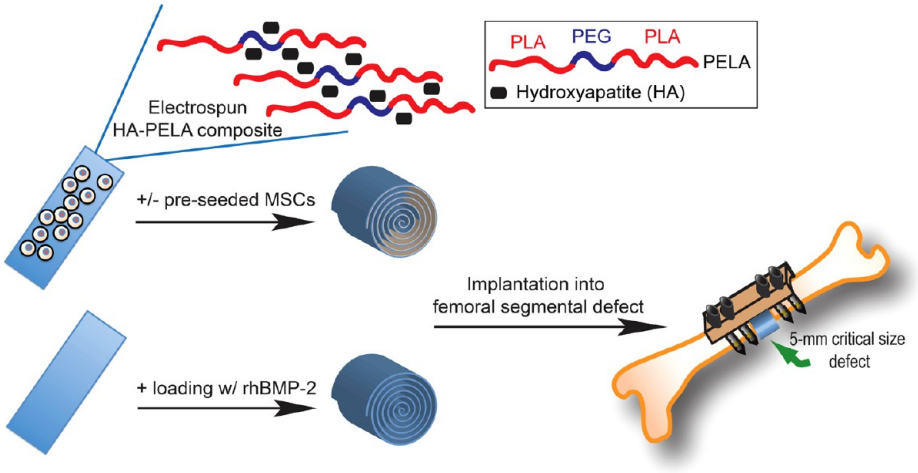

when the hydrophilic HA was poorly dispersed with hydrophobic biodegradable polymers such as poly(lactic acid) (PLA) and poly(ε-caprolactone) (PCL), the inadequate interfacial adhesion could result in HA aggregation and mechanical failure at the polymer−HA interface. This leads to deterioration of the mechanical and handling properties as well as inconsistent biological performance of the resulting composite scaffold.[12−14]

Gas plasma treatment, addition of surfactants, and surface modification of HA have all been used to improve the interfacial adhesion of HA with hydrophobic polymers with varied successes. Gas plasma treatment of electrospun PCL scaffolds increased hydrophilicity and improved the adhesion of human fetal osteoblasts[15] but did not result in a statistically significant improvement in scaffold mineralization. In critical-size calvarial defects in rats, oxygen gas plasma-treated electrospun PLA scaffolds coated with bioglass and HA were shown to support more effective new bone formation (∼70% fill) than PLA alone, HA−PLA, or PLA with tricalcium phosphate.[16] Disadvantages to the plasma treatment approach include potential disruption of scaffold morphology, limited treatment penetration depth, and the transient nature of the surface modification due to molecular motion.[17] Surfactants and silane coupling reagents have been used to disperse HA with PLA for the preparation of electrospun composites;[18,19] however, the biocompatibility of these approaches is unclear.[20] Poly(lactic acid-*co*-glycolic acid) (PLGA) scaffolds containing HA surface grafted with PLA resulted in lower levels of calcium deposition than unmodified HA when implanted intramuscularly in rabbits.[21]

With the goal of achieving well-integrated polymer−HA composites without surface-modification of the scaffold or HA itself, we recently developed the biodegradable amphiphilic triblock copolymer poly(D,L-lactic acid)-*co*-poly(ethylene glycol)-*co*-poly(D,L-lactic acid) (PELA).[7] The hydrophilic poly(ethylene glycol) (PEG) was chosen as the center block to enable the dispersion and binding with the hydrophilic HA mineral, while the hydrophobic PLA blocks provided biodegradability and aqueous stability. The chosen molecular weight of the PEG block was 20 kDa, facilitating bioresorption and renal clearance.[22] The high molecular weight (120 kDa) of PELA copolymer enabled polymer entanglements for facile electrospinning. The electrospun HA−PELA composites supported far more potent osteogenic gene expression of rat bone marrow derived stromal cells (MSCs) in vitro than conventional electrospun HA−PLA composites.[7] For example, little or no differences in mRNA expression of early- or late-stage osteogenesis markers (RUNX2 or osteocalcin) were observed when adding calcium-deficient HA to electrospun PLLA scaffolds.[11] Similarly, little change in gene expression was observed when culturing human embryonic stem cell-derived MSCs on PLLA/PLGA scaffolds with varying HA contents.[23] By contrast, the expression of osteopontin and osteocalcin was over 2 orders of magnitude higher for MSCs cultured in osteogenic medium for 2 weeks on HA−PELA than conventional HA−PLA. This enhanced bioactivity of electrospun HA−PELA may be due to the uniform presentation of HA to adhered cells and due to the increased bioactivity of proteins adhered to amphiphilic polymers,[24−26] such as PELA, compared to hydrophobic polymers such as PLA. Meanwhile, we also observed high elasticity (>200% ultimate strain), superhydrophilicity (water contact angle ≈ 0°), and hydration-induced stiffening (with storage modulus increased from 2 to ∼25 MPa) of the HA−PELA composite.[7] These unique physical properties, a result of the stable HA integration and the dynamic phase- separation of the amphiphilic blocks,[7] are in stark contrast to the brittleness, low aqueous wettability, and deteriorating mechanical integrity upon wetting exhibited by conventional degradable polymer−mineral composites. HA−PELA-based scaffolds could address a number of major limitations of conventional bone tissue engineering scaffolds by enabling facile absorption of aqueous suspensions of cells and growth factors, easy surgical handling, and stable fixation upon implantation. The combination of enhanced bioactivity and handling characteristics makes the simple electrospun HA−PELA scaffolds uniquely suited for evaluating cell- and protein factor-based bone regeneration approaches and ultimate clinical translation for treating critical-size bone defects. However, whether these standalone bioactive electrospun composites can promote volumetric bone regeneration (particularly within critical-size long bone defects), a challenging clinical problem in orthopedic trauma care,[27] has not been explored.

Here we exploited the handling characteristics (hydrophilicity, elasticity) and in vitro bioactivity of electrospun HA−PELA in the form of 3-D spirals for augmenting the repair of critical-size long bone defects. We aimed to examine whether enhanced bioactivity in vitro translates to effective templated

DOI: 10.1021/am508984y
ACS Appl. Mater. Interfaces 2015, 7, 4890−4901

bone regeneration in vivo. We tested the overall hypothesis that electrospun bioactive scaffolds support osteogenesis through the action of exogenously seeded progenitor cells or through endogenous progenitor cells recruited to the scaffold with a low dose of osteoinductive growth factor. We tested this hypothesis by comparing the performance of spiral-wrapped HA−PELA scaffolds with or without preseeded MSCs to scaffolds loaded with a low dose of rhBMP-2 (500 ng) in healing 5 mm critical-size femoral segmental defects in rats (Scheme 1). We first validated the feasibility of delivering exogenous progenitor cells and growth factors via electrospun HA−PELA by tracking the survival of labeled cells in vivo and the release profile of bioactive rhBMP-2 in vitro, respectively. Bone formation supported by the scaffolds in each treatment group was longitudinally monitored using X-ray radiography and quantitative in vivo microcomputed tomography (μ-CT). The morphology of bone formation, particularly immature bone, and the immune response to the scaffold degradation byproducts was assessed using end-point histology.

2. MATERIALS AND METHODS

2.1. Scaffold Fabrication. PELA was synthesized and electrospun with HA as previously described.[7] Briefly, PELA was synthesized by ring-opening polymerization of 3,4-dimethyl-1,4-dioxane-2,5 dione (D,L-Lactide; Sigma-Aldrich, St. Louis, MO) initiated by PEG (20 000 Da; Fluka BioUltra, Switzerland) and catalyzed by Sn(II) 2-ethylhexanoate (500 ppm; Sigma-Aldrich, St. Louis, MO). The resulting polymer (MW 131 800 Da, PDI 1.43) was dissolved in chloroform, purified by precipitation in methanol, and dried in a vacuum oven. Polycrystalline HA powder (consisting of loose aggregates of ∼100 nm crystallites) was purchased from Alfa Aesar (Ward Hill, MA). The HA (10 wt %) was bath sonicated in 5 mL of 1:4 (v/v) dimethylformamide/chloroform for 30 min prior to the addition of PELA (1.25 g, 25% w/v). The mixture was stirred overnight at room temperature. The suspension was then electrospun at a rate of 1.7 mL h^{-1} with a syringe pump (Orion Sage M361; Thermo Scientific, Billerica, MA) through a 22 G needle at 12 kV (supplied by a high-voltage power supply from Gamma High Voltage Research, Ormond Beach, FL) onto a grounded aluminum collector positioned 15 cm away. HA−PELA scaffolds with a thickness of 0.10−0.20 mm were obtained after 2 h of electrospinning. The scaffolds were dried in a vacuum oven at room temperature for 48 h to remove any residual solvent and stored in a desiccator at 4 °C prior to use.

2.2. Rat Bone Marrow Stromal Cell (MSC) Isolation. MSCs were isolated from the long bones of 4 week old male Charles River SASCO SD rats according to the protocol approved by the University of Massachusetts Medical School Institutional Animal Care and Use committee, as previously described.[28] Bone marrow was flushed with cold minimal essential medium (αMEM; Life Technologies, Carlsbad, CA). Prior to plating, red blood cells were lysed with sterile water, cells were resuspended in MSC expansion medium (αMEM without ascorbic acid, supplemented with 20% fetal bovine serum, 2% L-glutamine, and 1% penicillin−streptomycin), and passed through a sterile strainer. Nonadherent cells were removed after 4 days of culture, and the remaining adherent cells were expanded until 70% confluence prior to use.

2.3. Scaffold Preparation. Scaffolds were sterilized by exposure to UV light (254 nm) for 30 min on each side and equilibrated overnight in MSC expansion medium prior to use. For MSC-loaded scaffolds, 100 000 MSC/cm^2 in a 50 μL expansion medium were seeded onto scaffolds (5.3 mm × 40 mm × 0.10−0.12 mm) which were placed in 6-well ultralow cell attachment plates (Corning Inc., Corning, NY). Following 30 min of incubation (37 °C, 5% CO_2), 2 mL of expansion medium was added to the wells and the scaffolds were incubated for an additional 24 h. Scaffolds were washed 3 times with PBS prior to implantation. Cell-free and rhBMP-2-loaded scaffolds were processed in the same manner but without MSCs. Loading of rhBMP-2 (CHO-derived; R&D Systems, Minneapolis, MN; 500 ng in 50 μL PBS) was performed 15 min prior to implantation.

2.4. MSC Attachment and Viability on Spiral-Wrapped HA−PELA. MSCs were seeded onto electrospun HA−PELA scaffolds as described above. After 24 h, scaffolds were spiral wrapped into 3-D cylinders or cultured on unperturbed electrospun meshes in the ultralow attachment 6-well plates. At each time point, fresh medium containing 9% (v/v) Cell Counting Kit-8 reagent (CCK-8; Dojindo Molecular Technologies Inc., Japan) was added to the wells. After 4 h incubation, 100 μL of medium was removed for measurement of absorbance at 450 nm with 650 nm background correction on a Multiskan FC microplate photometer (Thermo Scientific, Billerica, MA). The remainder of the medium was aspirated, the scaffolds were washed with PBS, and medium was replaced for continued culture up to 14 days. The CCK-8 assay was carried out at day 1, 7, and 14. Following the 14-day culture, the spiral-wrapped scaffolds were unwrapped and the adherent cells were labeled with Alexa Fluor 488 Phalloidin and DAPI (Life Technologies, Carlsbad, CA) and imaged on an inverted epifluorescence microscope (Ziess Axiovert 40 CFL; Carl Ziess, Germany).

2.5. In Vitro rhBMP-2 Release from HA−PELA. Electrospun HA−PELA scaffolds (n = 3) were punched into 0.32 cm^2 circles, sterilized 30 min/side with UV, and equilibrated overnight in deionized water at 37 °C. They were then air dried in a biosafety cabinet, placed in ultralow attachment 24-well plates (Corning Inc., Corning, NY), and loaded with 75 ng rhBMP-2 in 5 μL of PBS. One milliliter of PBS was then added to each well, and the plate was incubated at 37 °C. For each time point, the release buffer (1 mL) was collected and replenished with fresh PBS. The release buffer was frozen and stored at −80 °C prior to rhBMP-2 measurement. At the end of the release experiment, all collected release buffers were thawed and the rhBMP-2 concentration was determined using a rhBMP-2 ELISA kit (R&D Systems, Minneapolis, MN).

2.6. In Vitro Bioactivity of rhBMP-2 Retained on HA−PELA Following 7-Day Incubation in PBS. The HA−PELA scaffolds, retrieved after 7 day PBS incubation from the BMP-2 release study, were then assessed for their ability to support C2C12 trans-differentiation in order to confirm the osteogenic bioactivity of the rhBMP-2 retained on the scaffolds. C2C12 cells were seeded directly onto the scaffolds (20 000 cells/cm^2) that were placed in ultralow attachment 96-well plates (Corning Inc., Corning, NY) and cultured in DMEM containing 5% fetal bovine serum and 1% penicillin−streptomycin for 72 h. The scaffolds were fixed in periodate-lysine-paraformaldehyde (PLP) fixative,[29] and alkaline phosphatase (ALP) activity was stained using a Leukocyte Alkaline Phosphatase Kit (Sigma-Aldrich, St. Louis, MO). Following staining, the scaffolds where imaged on an inverted microscope (Ziess Axiovert 40).

2.7. In Vivo Study Design and Surgical Procedure. Electrospun HA−PELA alone (n = 12), preseeded with MSCs (n = 11), or loaded with rhBMP-2 (n = 11) were rolled into 5.3 mm long and 3 mm wide spirals and press fit into 5 mm segmental femoral defects in rats. Bone healing was monitored over time by in vivo μ-CT every 4 weeks and also radiographed every 2 weeks. Animals were sacrificed at 4 or 12 weeks for histology (n = 2 per treatment group/time point). A subset of animals was sacrificed at 12 weeks for torsion testing (n = 4 for HA−PELA with preseeded MSCs; n = 7 for HA−PELA with rhBMP-2). In order to track the fate of transplanted MSCs, a subset of animals received scaffolds seeded with green fluorescent protein (GFP)-transduced MSCs and were sacrificed at 2 days, 7 days, or 4 weeks post-op for histology (n = 2).

All animal procedures were approved by the University of Massachusetts Medical School Institutional Animal Care and Use Committee. Male Charles River SASCO SD rats (290−300 g) were sedated with 5% isoflurane−oxygen and maintained at 2% isoflurane−oxygen during surgery. A 5 mm critical-sized femoral defect was created and stabilized with a polyetheretherketone (PEEK) fixation plate as previously described.[30] Briefly, the femur was exposed by a combination of sharp and blunt dissection. The periosteum was circumferentially removed in order to emulate a challenging healing environment. A PEEK fixation plate was secured with 2 stainless steel

DOI: 10.1021/am508984y
ACS Appl. Mater. Interfaces 2015, 7, 4890−4901

bicortical screws flanking each side of the defect and with the two immediately adjacent to the defect further stabilized with hex nuts. The 5 mm defect was created with an oscillating Hall saw, and bone debris was removed by copious irrigation with sterile saline. The empty, MSC-loaded, or rhBMP-2 loaded spiral wrapped scaffolds were then fit into the defect. The wounds were closed with sutures, and the rats were given cefazolin (20 mg/kg, once per day) and buprenorphine (0.08 mg/kg, every 8 h) subcutaneously for 2 days. Rats were radiographed immediately following surgery to confirm proper PEEK plate fixation.

2.8. Microcomputed Tomography (μ-CT). Every 4 weeks following surgery, animals were sedated and maintained with 2% isoflurane−oxygen for scanning of the femurs on a Scanco vivaCT 75 μ-CT system (Scanco Medical, Switzerland) at a voxel size of 30 × 30 × 30 μm^3. Scans were also performed on 12 week explants with the same scanning resolution. The center of the defect and surrounding cortical bone was located based on the bicortical screws flanking the defect. From the defect center, a total of 83 30 μm slices from each side were included to construct the region of interest (ROI) within the defect site, totaling 5.01 mm in length, for analysis. A global threshold was applied to remove soft tissue and scaffold background for quantification and reconstructing 3-D images. Bone volume and bone mineral density within the ROI were calculated using Scanco Medical's 3D analysis software.

2.9. Histology. Explants were fixed in PLP fixative[29] at 4 °C for 2 days and subsequently decalcified in 18% aqueous ethylenediaminetetraacetic acid (EDTA) (pH 8.0) for 4 weeks with exchanges of fresh EDTA solution twice a week. Following removal of the PEEK fixation plates, the explants were subjected to serial dehydration, paraffin embedding, and sectioning. Six micrometer thick sections were stained by hematoxalyin and eosin (H&E) or toluidine blue. As with the μ-CT imaging, the defect site and surround cortical bone was located by the bicortical screws flanking the defect. The position of the screws and the 5 mm defect size reproducibly created using the double-bladed oscillating saw within the space defined by the flanking screws allowed for the differentiation of the cortical bone surrounding the defect from the new bone formed within/over the defect.

2.10. Lentiviral GFP Transduction of MSCs and Tracking of Implanted GFP-MSCs. MSCs were transduced with lentiviral vectors (Cellomics Technology, Halethorpe, MD) expressing enhanced GFP driven by cytomegalovirus (CMV), elongation factor-1 alpha (EF1α), or ubiquitin C (UBC) promoters. Cells were transduced with the virus at a multiplicity of infection of 5, 25, or 50. Passage 1 MSCs were seeded at a density of ∼10 000 cells/cm^2 in transduction medium (αMEM, 20% heat-inactivated FBS, 1% L-glutamine) and cultured for 24 h before the respective lentiviral vectors were added. The culture plates were spun for 30 min in a centrifuge (1200 × g, 32 °C) to increase transduction efficiency before being subjected to continued culture for 24 h in transduction medium. The medium was then changed to MSC expansion medium, and the cells were cultured for an additional 24 h prior to use. Transduction efficiency (% of cells transfected as revealed by green fluorescence) was examined by epifluorescence microscopy (Zeiss Axiovert 40 CFL) in 3 randomly selected fields of view at 100× magnification.

In order to track the viability of MSCs seeded on the scaffold and implanted in the rat femoral segmental defect, GFP-MSCs were seeded on HA−PELA as described above. One of the GFP-MSC-seeded scaffolds, prepared at the same time as the scaffolds to be implanted, was rinsed with PBS and imaged on a fluorescent microscope (Zeiss Axiovert 40 CFL) to obtain preimplantation GFP signal control. Remaining scaffolds were wrapped into 3-D cylinders and implanted into the rat critical size femoral defects as described above. At 2 days, 7 days, and 4 weeks post-op, animals were sacrificed and the scaffolds were excised from the defects, carefully unwrapped, and mounted on a microscope slide for GFP imaging.

Immunohistochemical staining was used to track GFP-MSCs at 4 weeks post-op. Explants were fixed, decalcified, and processed for histology as described above. The sections were deparaffinized, unmasked in 10 mM sodium citrate buffer (pH 6.0), and treated with rabbit polyclonal GFP antibody (#2555; Cell Signaling Technology, Danvers, MA) in SignalStain Antibody Diluent (Cell Signaling Technology). SignalStain Boost (Cell Signaling Technology) was used for detection of the rabbit antibodies. SignalSlide GFP IHC controls (Cell Signaling Technology) were used as positive controls.

2.11. Statistical Analysis. All statistical analysis was performed with Prism 6.0 (GraphPad Software Inc., La Jolla, CA). Grubbs' testing (alpha = 0.05) identified one outlier in the μ-CT quantification of the HA−PELA group, which was removed from subsequent analyses. Shapiro-Wilk testing confirmed that the data in all groups followed a normal distribution. One-way analysis of variance (ANOVA) with Tukey posthoc testing was thus used for all statistical comparisons.

3. RESULTS

3.1. MSC Attachment and viability. MSCs readily adhered to the HA−PELA scaffolds. Although cell viability was significantly reduced (by 30%) at 24 h post spiral wrapping, comparable numbers of viable cells were present on flat and spiral-wrapped scaffolds by 7 and 14 days in culture (Figure 1A). MSCs adhered on scaffolds after 14 days in culture were

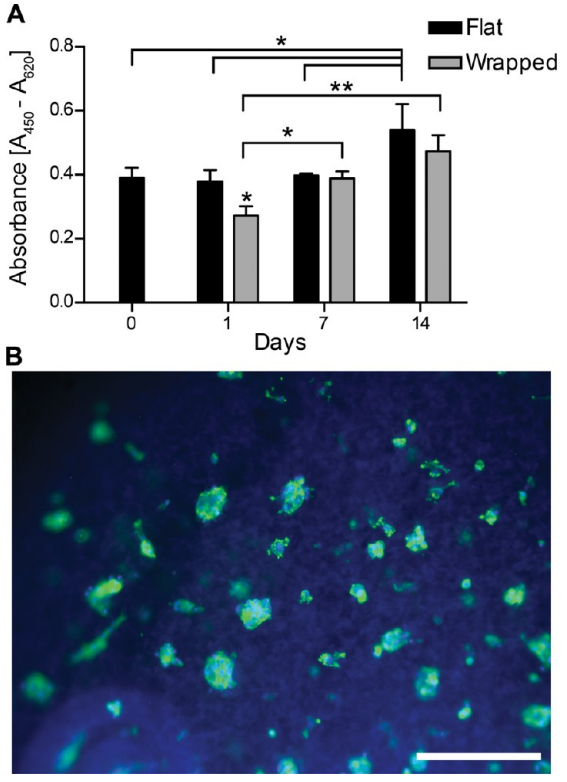

Figure 1. Viability of MSCs adhered to flat and spiral-wrapped HA−PELA scaffolds over time. (A) CCK-8 cell viability over 14 days. Day 0 cell viability was determined prior to spiral wrapping the scaffolds: (*) $p < 0.05$, (**) $p < 0.01$ (ANOVA with Tukey posthoc). (B) Actin staining of adhered MSCs on the spiral-wrapped scaffold after 14 days in culture. Scale bar = 250 μm.

visualized by F-actin (fluorescent phalloidin) and nuclei (DAPI) staining (Figure 1B). Substantial nonspecific absorption of DAPI onto the electrospun scaffold was observed.

3.2. Tracking GFP-Labeled MSCs in Vivo. We compared the labeling efficacy of GFP driven by cytomegalovirus (CMV), elongation factor 1-alpha (EF1α), and ubiquitin C (UBC) promoters at three multiplicities of infection (MOI; 5, 25, 50) to optimize lentiviral GFP transduction of MSCs. CMV and EF1α promoters resulted in the highest levels of GFP signal with high labeling efficiency (>90%) (Figure S1A, Supporting

DOI: 10.1021/am508984y
ACS Appl. Mater. Interfaces 2015, 7, 4890−4901

Information). EF1α-GFP at an MOI of 25 was chosen for all subsequent MSC labeling due to the uniform GFP signal, low cytotoxicity (Figure S1B, Supporting Information), and minimal effects on cell proliferation (Figure S1C, Supporting Information). There was no significant compromise in the potency of induced osteogenic or adipogenic differentiations of the MSCs upon GFP labeling (Figure S1D–G, Supporting Information).

GFP-labeled cells were seeded on HA–PELA and implanted in the 5 mm femoral segmental defect, and their fate was tracked over 4 weeks post-implantation. GFP-MSCs remained detectable on the scaffold at 2 and 7 days after implantation (Figure 2) as shown by fluorescent microscopy, although the

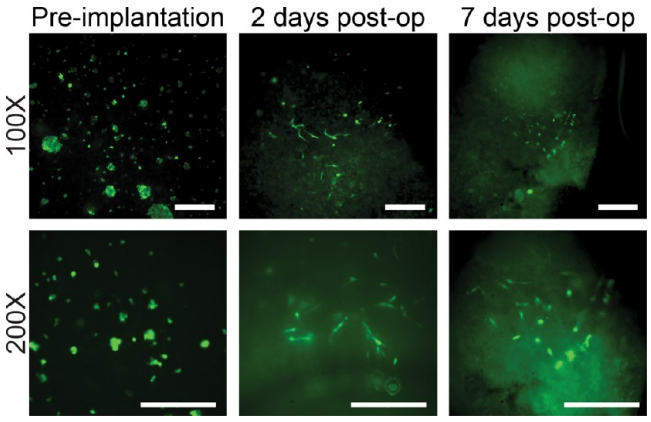

Figure 2. Fluorescence microscopy of GFP-labeled rMSCs adhered to HA–PELA scaffolds before and after implantation. Scale bars = 300 μm.

number of GFP-positive cells decreased over time. Morphology of the GFP-labeled cells attached to the scaffolds changed from a rounded shape preimplantation to a more extended/spindle shape, supporting their adhesion and spreading on the osteoconductive scaffolds. No labeled cells were detected at 4 weeks post-op by immunohistochemistry (IHC) with anti-GFP antibodies (data not shown).

3.3. Retention and Release of rhBMP-2 from HA–PELA. A slow yet sustained release of rhBMP-2 from the HA–PELA scaffold was detected by ELISA over 72 h (Figure 3A). Only ~10% of the rhBMP-2 absorbed to the scaffold was released within the first 24 h, and a cumulative 12% was released by 72 h. The rhBMP-2 retained on the scaffolds remained bioactive and was able to induce the osteogenic transdifferentiation of C2C12 myoblasts, as evidenced by the positive staining for osteogenic marker ALP of the C2C12 cells cultured on the scaffold preloaded with rhBMP-2 and subjected to a 7 day prior incubation in PBS (Figure 3B). ALP staining was not detected with the cells cultured on the scaffold without rhBMP-2 loading.

3.4. Radiographic Follow-up of Implanted Spiral-Wrapped HA–PELA with/without Preseeded MSCs or rhBMP-2. HA–PELA scaffolds, with or without preseeded MSCs or absorbed rhBMP-2, were manually wrapped into cylindrical spirals (Figure 4A) and implanted into 5 mm rat femoral defects (Figure 4B). The implanted scaffolds could not be readily visualized by post-op X-ray radiographs due to the relatively low density of the HA (10 wt %) within the HA–PELA scaffold (Figure 4C). The untreated defect remained unfilled by 12 weeks post-op as revealed by X-ray radiography

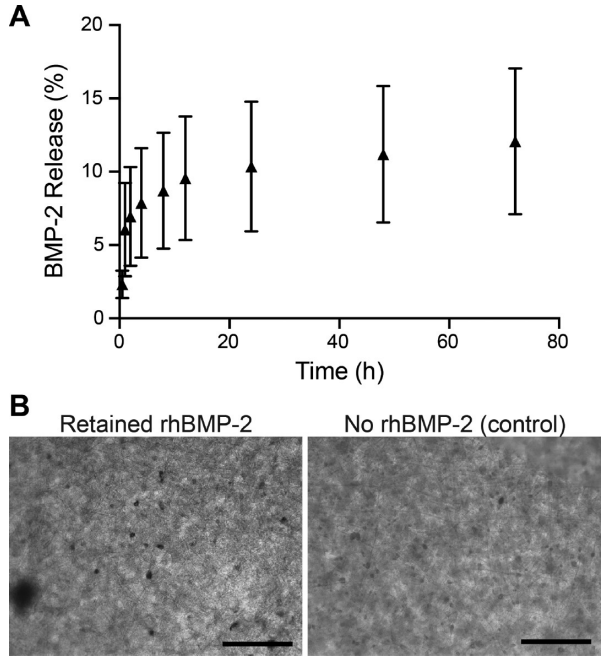

Figure 3. (A) Cumulative percentage of rhBMP-2 (75 ng loading dose) released from HA–PELA (n = 3) in PBS at 37 °C. (B) Alkaline phosphatase staining of the C2C12 myoblasts cultured on HA–PELA with or without preabsorbed rhBMP-2 for 3 days. The scaffolds bearing 75 ng of rhBMP-2 were incubated in PBS for 7 days before being retrieved and seeded with C2C12 cells. Scale bars = 250 μm.

(Figure 4C), confirming that the 5 mm defect was indeed a critical-size defect. New bone formation was visible by radiography in all treatment groups by 12 weeks post-op (Figure 4C). The greatest amount of bridging bony callus was detected in the groups treated with HA–PELA and 500 ng of rhBMP-2. Of note, for the group treated with HA–PELA and MSCs, the new bone formation appeared to have occurred within, instead of surrounding the outer surface of, the spiral-wrapped scaffold.

3.5. Histological Evaluation of the Cellularity and New Bone Formation within and Surrounding the HA–PELA Scaffold with/without MSCs or rhBMP-2. Histological sections were cut longitudinally, revealing the new bone/scaffold morphology across the length of the 5 mm defect (Figure 5A). Additional high-magnification images of the center of the scaffolds, allowing easier identification of new bone, scaffold degradation, blood vessel formation, and immune cell penetration are shown in Figure S2, Supporting Information. HA–PELA scaffolds remained visible in all treatment groups by 12 weeks, in agreement with our prior in vitro degradation data (~80% scaffold mass remaining after 12 weeks in PBS at 37 °C)[7] (Figure 5B). Immune cells infiltrated within these HA–PELA scaffolds consisted primarily of macrophages and foreign body giant cells (askterisk (*), Figure 5B). No lymphocytes, neutrophils, eosinophils, or mast cells that would have suggested acute inflammatory responses or allergic reactions were detected. Consistent with this mild local immune response, the implantation of HA–PELA also did not lead to gross changes to vital/scavenger organs by up to 24 weeks post-implantation (Figure S3, Supporting Information).

Substantial new bone formation at the scaffold/cortical bone interface, accompanied by neovessel formation (arrowheads, Figure 5B), was readily detected in all treatment groups by 12

DOI: 10.1021/am508984y
ACS Appl. Mater. Interfaces 2015, 7, 4890–4901

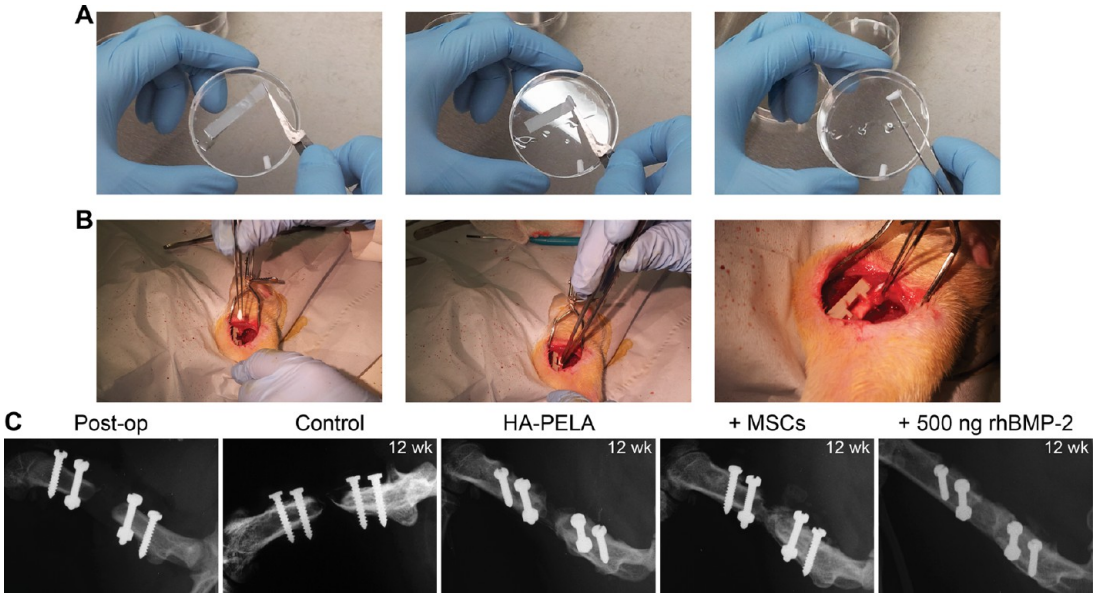

Figure 4. Spiral wrapping and surgical implantation of HA−PELA scaffolds and post-op radiographical follow-ups of the site of implantation. (A) Wrapping HA−PELA scaffolds into cylindrical spirals prior to surgery. (B) Implantation of spiral-wrapped HA−PELA scaffolds into 5 mm rat femoral segmental defects. (C) Radiographs of the scaffold-filled defect immediately post-op, untreated control defect after 12 weeks, and scaffold-filled defects after 12 weeks.

weeks (visible as early as 4 weeks) as revealed by H&E and polarized light microscopy. The new bone formed within the HA−PELA scaffolds, however, differed significantly in both morphology and maturity among the 3 treatment groups. The new bone formed within the bare HA−PELA scaffold was randomly aligned and remained immature by 12 weeks as reflected by the lack of strong birefringence under polarized light. By contrast, the new bone formed at the center of the scaffold preseeded with MSCs was directly templated by and encapsulated between adjacent scaffold layers. The new bone formation templated by MSC-seeded HA−PELA, however, was still characterized with a weak birefringence at 12 weeks. New bone formation was also visible within the HA−PELA scaffold absorbed with rhBMP-2, although they did not appear to be clearly templated by the spiral-wrapped scaffold morphology. With the delivery of rhBMP-2, strong birefringence at both the cortical−scaffold junction and along the outer periphery of the scaffold indicative of aligned collagen fibers and more mature bone was observed under polarized light. Finally, purple toluidine blue staining for cartilaginous matrix was detectable in all areas of new bone formation, most notably at the cortical bone−scaffold junctions, in all treatment groups.

3.6. μ-CT Analyses. Bone mineral density mapping of the longitudinal and axial center slices of the reconstructed ROI at 4 and 12 weeks post-op was used to visualize the morphology and maturity the new bone formed around/within the scaffold-filled defects over time (Figure 6). Density maps of the implanted HA−PELA scaffold immediately post-op confirmed that the HA within the scaffold is not visible with the density thresholds used for imaging (Figure 6). The color mapping revealed that new bone formed at the scaffold/cortical bone interface and within the scaffold-filled defect in all treatment groups after 4 weeks. Most robust and mature bone formation was observed with the group absorbed with rhBMP-2, with the recanalization of the new bone clearly visible at 12 weeks. More robust new bone appeared to be localized on the side opposite the PEEK fixation plate. In the absence of rhBMP-2, bone formation was clearly templated by the spiral-wrapped scaffolds in both the HA−PELA alone and HA−PELA + MSCs groups. The templated new bone growth in these treatment groups was visualized as the vertical lines and concentric lines in the longitudinal and axial color maps, respectively. Maturation of the new bone from 4 to 12 weeks was observed for all groups, as evidenced by the increased red color in the mineral density color mapping.

Reconstructed 3-D μ-CT images confirmed the bony callus formation at the graft−cortical bone interface and some degrees of scaffold-templated growth toward the center of the defect in the HA−PELA alone group (Figure 7A). Greater amounts of scaffold-templated new bone formation were visible at the center of the defect by 12 weeks with preseeded MSCs, consistent with X-ray radiograph observations (Figure 4C). The most robust bony callus formation bridging over the defect was observed with the HA−PELA + rhBMP-2 treatment group. Bone volume and bone mineral density in all treatment groups increased over the 12-week post-op monitoring period (Figure 7B and 7C). The HA−PELA + rhBMP-2 group resulted in significantly greater bone volume than HA−PELA alone or HA−PELA + MSCs at both 4 and 12 weeks post-op (Figure 7B). There was no significant difference in bone mineral density among the three treatment groups at a given time point examined (Figure 7C).

4. DISCUSSION

We hypothesized that a spiral-wrapped bioactive electrospun scaffold would potentiate the ability of exogenously seeded progenitor cells or endogenous cells recruited with a low dose of rhBMP-2 to repair long bone defects. To test this hypothesis, we used a 5 mm rat femoral segmental defect which has been validated as a critical-size long bone defect model to test the performance of bone tissue engineering scaffolds by our group, as shown in Figure 4C, and others.[30−33] The critical size of the defect, coupled with the removal of the surrounding periosteum, serves to emulate a challenging clinical scenario[34]

DOI: 10.1021/am508984y
ACS Appl. Mater. Interfaces 2015, 7, 4890−4901

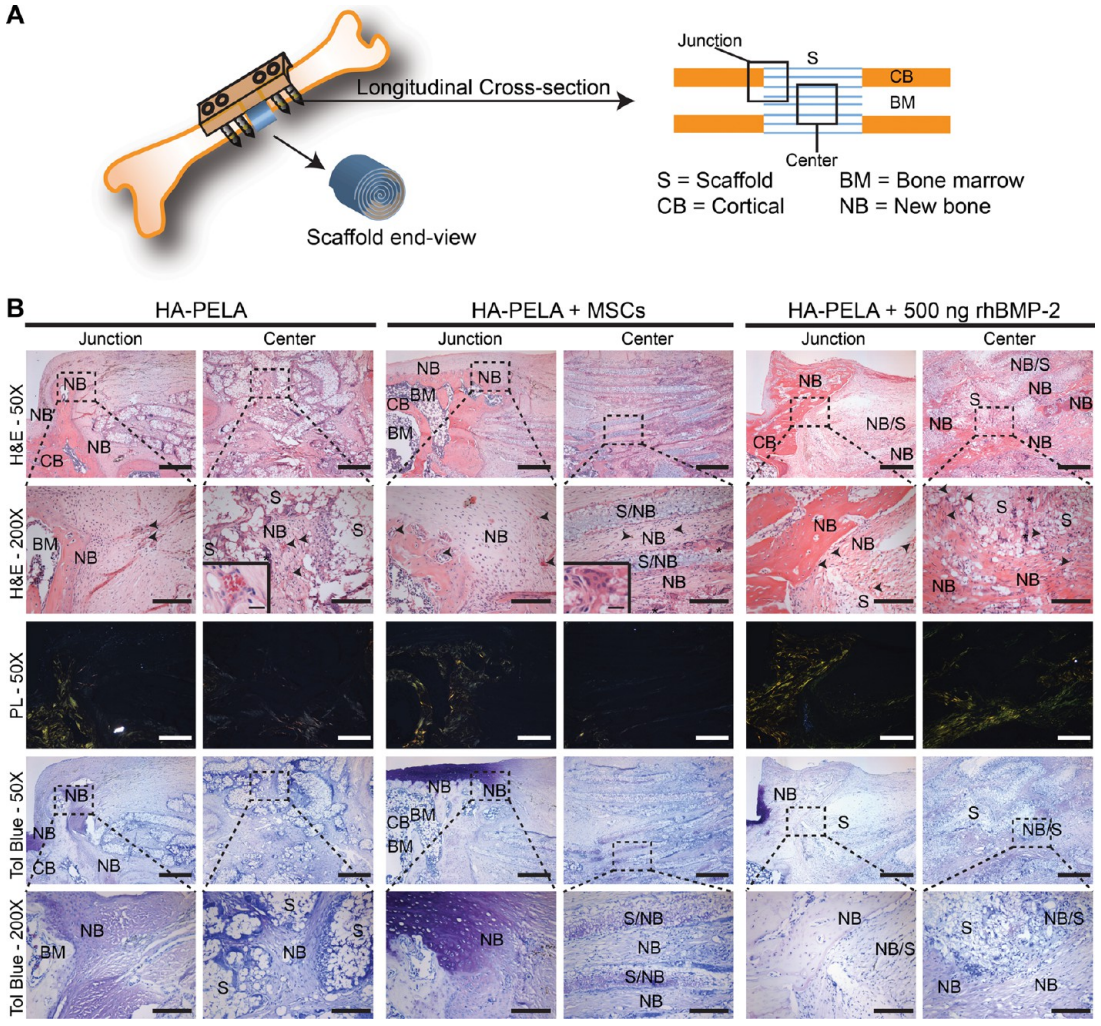

Figure 5. Histological analysis of cellular infiltration and bone formation within/around the scaffold-filled defect at 12 weeks post-op. (A) Schematic of the histological sectioning along the longitudinal direction to enable examination of new bone formation across the full length of the defect. (B) Bright field and polarized light (PL) micrographs of hematoxlyn and eosin (H&E) and toluidine blue (Tol Blue) stained sections. For each treatment group (HA−PELA, HA−PELA + MSCs, and HA−PELA + rhBMP2), images were taken both at the cortical bone−scaffold junction and within the center of the scaffold. Arrowheads indicate blood vessels and asterisk (*) indicates macrophages/foreign body giant cells. Scale bar = 500 μm for micrographs taken at 50× magnification and 150 μm for those taken at 200× magnification. Inset images show a representative blood vessel in the HA−PELA group and a representative foreign body giant cell in the HA−PELA + MSCs group. Inset scale bars = 20 μm.

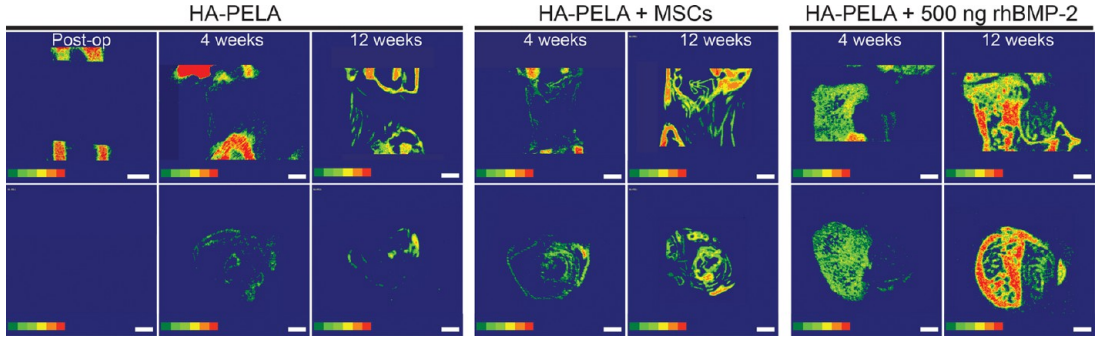

Figure 6. Two-dimensional bone mineral density color maps of the scaffold-filled defect over time (red representing higher mineral density). Longitudinal (top) and axial (bottom) midslices of the defect treated with HA−PELA immediately post-op, and HA−PELA, HA−PELA + rMSCs, and HA−PELA + 500 ng rhBMP-2 at 4 and 12 weeks post-op. Scale bars = 1 mm.

precluding healing without proper intervention.[35] In our prior work we demonstrated that the handling properties (aqueous wettability and stability, tensile elasticity) and bioactivity (osteoconductivity and osteoinductivity) of electrospun degradable polymer/HA composites can be significantly improved by using an amphiphilic PELA block copolymer instead of the conventional hydrophobic PLA.[7] Here we demonstrated that these handling and bioactivity characteristics

DOI: 10.1021/am508984y
ACS Appl. Mater. Interfaces 2015, 7, 4890−4901

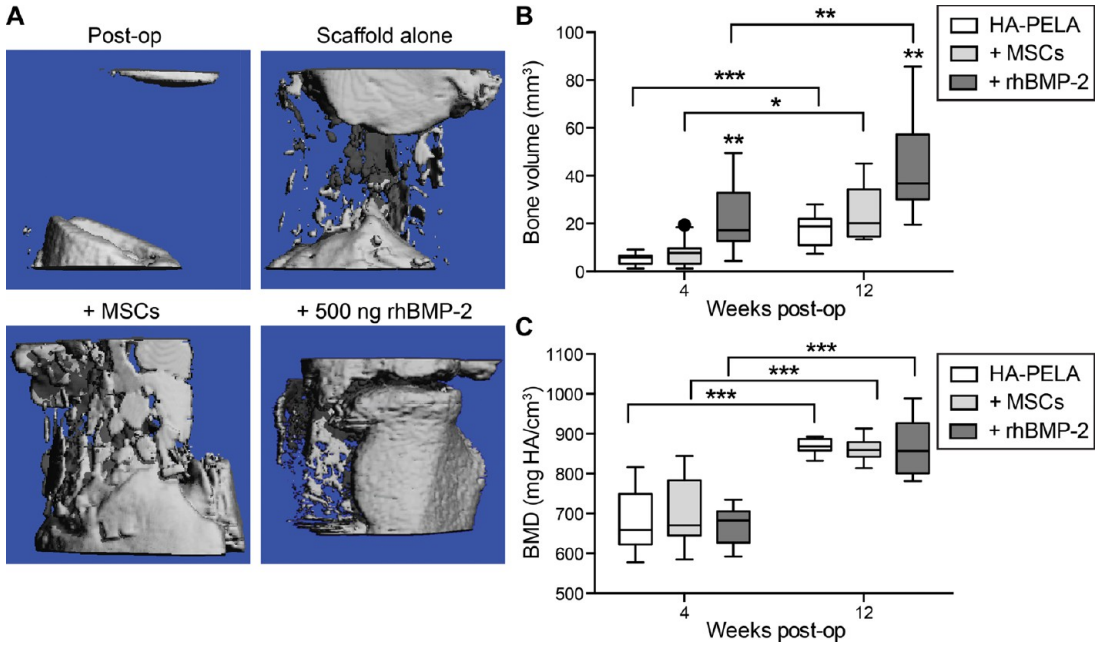

Figure 7. In vivo μ-CT monitoring of the scaffold-filled defects over time. (A) μ-CT 3-D reconstructions of the ROI immediately post-op and those containing HA−PELA, HA−PELA + rMSCs, or HA−PELA + rhBMP-2 at 12 weeks post-op. Extra slices from the adjacent cortical bone were included for the reconstruction of the post-op ROI for convenient visual reference. For all treatment groups at 12 weeks, only the 5 mm defect site is shown. Global thresholding was applied to exclude the HA−PELA scaffold within the defect. (B−C) μ-CT quantification of new bone volume (mm^3) and bone mineral density (BMD; mg HA/cm^3) in the ROI at 4 and 12 weeks post-op. Data are graphed as Tukey box and whisker plots where whiskers represent the lower and upper 1.5 interquartile ranges (IQR). Data points outside the 1.5 IQR are plotted as individual points: (*) $p < 0.05$, (**) $p < 0.01$, (***) $p < 0.001$.

made electrospun HA−PELA uniquely suited for the spiral-wrapped scaffold-templated bone regeneration strategy.

Spiral-wrapping the electrospun HA−PELA scaffolds enabled us to take advantage of both the high surface area of electrospun materials to deliver therapeutics/support cellular adhesion and the defined 3-D configuration of the spiral to guide the cell-mediated regeneration of critical long bone defects. Furthermore, the relatively low quantity of polymer used to fabricate electrospun materials may also mitigate potential adverse immune responses to the degradation products of bulk degradable polymer scaffolds.[36] Spiral-wrapped scaffolds in combination with other materials have been studied for potential tissue engineering applications in vitro.[37−41] Zhang et al. and Wang and Xu described spiral-wrapped electrospun PCL/salt-leached PCL film composites and electrospun PCL/sintered PLGA scaffolds, respectively,[39−41] although neither design was tested in vivo. Jiang et al. employed an electrostatic assembly strategy to fabricate a spiral-wrapped membrane composed of chitosan/cellulose/HA and tested their performance in augmenting the repair of rabbit radius defects.[37] However, the noncritical defect size they employed makes the efficacy of the scaffold difficult to interpret as the no-scaffold defect control also healed. Piskin et al. used spiral-wrapped electrospun PCL scaffolds containing simvastin to aid the healing of calvarial defects in rats; however, defect closure was not achieved by 6 months post-op.[38] Tubular electrospun scaffolds and flat electrospun membranes have also been used for containing soft hydrogels,[42,43] delivering platelet-rich plasma,[44] or guiding regeneration of nonweight-bearing cranial/mandibular defects.[45−48] Overall, in vivo studies that examine the efficacy of standalone 3-D electrospun scaffolds in a clinically relevant critical long bone defect model are lacking. Furthermore, a simple and scalable polymer and single-component scaffold design, such as as electrospun HA−PELA, is important to facilitate clinical translation.[3] By using spiral-wrapped HA−PELA as a standalone scaffold, we were able to evaluate its efficacy in delivering exogenous MSCs vs therapeutic proteins and how the simple bioactive electrospun scaffolds can guide bone formation in critical-size long bone defects without additional confounding variables.

We first demonstrated unequivocal feasibility of delivering exogenous MSCs via spiral-wrapped HA−PELA in vivo. Although it is believed that exogenous MSCs can improve bone formation in critical-size defects,[49−51] some studies fail to show statistically significant improvement in bone formation with cell-seeded constructs over cell-free constructs.[52] It is still under intense debate as to whether exogenous MSCs locally delivered to the defect site contribute to healing via paracrine effect (e.g., secreted factors) or by direct participation in osteo/chondral differentiation, with the former receiving more recent recognition.[53−55] Whereas literature reports on the fate of transplanted MSCs vary, most suggest that implanted exogenous cells have a limited lifetime within the defect site and do not substantially differentiate into osteoblast-like cells.[50,56,57] We believe that the biomaterial carrier plays an important role in determining the fate of the exogenous cells it delivers. We tested whether the bioactive electrospun HA−PELA scaffold could support MSC transplantation to the long bone defect. The hydrophilic surface and osteoconductive nature of HA−PELA allowed for easy loading of the MSC suspension and supported cellular adhesion and spreading (Figures 1B and 2). The elastic properties of HA−PELA facilitated the facile spiral wrapping of cell-laden HA−PELA. Manual rolling of the scaffold did not compromise the viability of the cells seeded on the scaffolds as revealed by in vitro monitoring of cell viability and proliferation over the course of

DOI: 10.1021/am508984y
ACS Appl. Mater. Interfaces 2015, 7, 4890−4901

14 days after the spiral wrapping (Figure 1). The relatively high cell seeding density of 100 000 cells/cm^2, which would have resulted in a confluent cell layer on tissue culture polystyrene, was chosen due to the relatively low cell seeding efficiencies of ∼35% on our electrospun scaffold. Future optimization of the cell seeding efficiency could potentially reduce the number of cells seeded.

Importantly, by tracking GFP-labeled MSCs, we showed that viable exogenous cells could still be detected up to 7 days post-implantation, although their number decreased over time (Figure 2). These cells also changed morphology from a rounded shape immediately after being seeded on HA−PELA to a spindle shape over time. Such an improved cell spreading is likely due to the absorption of endogenous cell-adhesive proteins from the tissue microenvironment onto the scaffolds. Agreeing with literature reports that exogenous cells seeded on a mineral-based carrier cannot be detected 14 days post subcutaneous implantation,[56] we also did not observe GFP-labeled rMSCs at later time points by IHC. While the persistence of viable transplanted cells at 7 days may support their direct participation in new bone formation, we were unable to determine their ultimate fate and contribution through the GFP-labeling approach.

Meanwhile, we demonstrated outstanding retention/release profile of rhBMP-2 on the electrospun HA−PELA, which established a clear benefit of HA−PELA for BMP-2 delivery. Although clinically used collagen sponge carriers absorbed with rhBMP-2 can be as effective as autografts for inducing new bone formation in some indications, particularly nonweight bearing ones,[58] they require loading doses of rhBMP-2 as high as 4.9 or 12.7 mg per graft,[59] compared to ∼5 μg/kilogram endogenous BMP-2 in natural bone.[60] Documented complications from such supra-physiologic doses rhBMP-2, which undergo burst release from the carrier (e.g., 100% released in vitro after 2 days),[32] include ectopic bone formation, inflammation, sexual dysfunction, and potentially cancer.[61,62] By contrast, although the expression of endogenous BMP-2 is the highest early during fracture healing in mice (at ∼1 day), its expression is sustained throughout the 21 day healing cascade, especially during the first week.[63] Thus, a more physiologically relevant delivery would require a scaffold capable of retention and sustained release of the osteogenic protein with preserved bioactivity over a reasonable time frame. The aqueous wettability of HA−PELA and high surface area of the well-integrated nanocrystalline HA (known for affinity for a wide range of proteins)[30] enabled facile loading and stable retention of aqueous rhBMP-2. The HA−PELA exhibited a slow yet sustained in vitro release of 10−15% of the loaded rhBMP-2 (235.8 ng/cm^2, same as the in vivo loading dose applied in this study) over the first 3 days (Figure 3A). Importantly, we also showed that the rhBMP-2 retained on the scaffold after 7 day incubation in PBS remained bioactive as evidenced by their ability to induce osteogenic transdifferentiation of adhered C2C12 myoblasts (Figure 3B).[64] The stable retention and sustained release of bioactive rhBMP-2, coupled with the previously reported bioactivity of HA−PELA, may facilitate the recruitment and differentiation of endogenous cells with a low rhBMP-2 dose, potentially mitigating clinical complications associated with the burst release of high doses of rhBMP-2.

We then investigated how combining these therapeutic modalities (exogenous cells or endogenous recruitment) with a bioactive electrospun scaffold could differentially augment the healing of critical-size rat femoral segmental defects. The spiral-wrapped HA−PELA scaffold, with a structure closely matching with that of the removed midshaft femoral segment, was press fit within the 5 mm segmental defect and remained stably fixed throughout the course of the 12 week study. The implanted scaffolds were still visible by histology at 12 weeks post-op (Figure 5), consistent with prior in vitro findings of ∼20% mass loss after 12 week incubation in PBS.[7] Macrophages and foreign body giant cells but no neutrophils or eosinophils were detected from the cells infiltrated in the scaffolds, consistent with a mild foreign body and immunogenic responses to HA−PELA and its degradation products and the lack of acute inflammation or allergic reactions.[65] Degradation-induced immune responses to PLA-based materials are well documented.[65,66] It has been hypothesized that calcium phosphate minerals including HA can buffer the acidic degradation products of PLA, thereby mitigating their immunogenicity.[67] It remains to be seen whether the mild local immune responses observed, partially attributed to the buffering effect of the 10 wt % HA incorporated into the amphiphilic scaffold, would be sustained when more complete degradation of the scaffold occurs at later time points.

All treatment groups, including the HA−PELA scaffold alone, facilitated new bone formation via an endochondral ossification mechanism within the defect site, as revealed by histology (Figure 5) and μ-CT analyses (Figures 6 and 7). The new bone formation observed in the HA−PELA alone group, particularly beyond the scaffold−cortical bone junction, supports the osteoconductivity of the scaffold.[30] The delivery of MSCs via the HA−PELA spiral resulted in a substantial increase in the new bone formed away from the cortical/implant junctions. In agreement with our hypothesis that the bioactive electrospun scaffold can support new bone formation by exogenous cells, the new bone appeared to be directly templated by the spiral-wrapped scaffold as confirmed by histology (Figure 5B) and μ-CT 2-D bone mineral density mapping (Figure 6). Such uniform distribution of new bone across the longitudinal span of the defect, concentrically separated by the spiral-wrapped electrospun scaffold and apparently promoted by the preseeded MSCs, has not been reported previously. Despite the unique morphology of the new bone, the delivery of MSCs alone did not result in significantly higher bone volume or bone mineral density than HA−PELA alone or complete bridging of the defect by 12 weeks (Figure 7B and 7C). The undegraded spiral-wrapped scaffold could have prevented the concentrically formed new bone from growing across the axial space and fusing together given the small pore size (1−10 μm) of electrospun materials.[68]

With an exceptionally low dose of rhBMP-2 delivered by HA−PELA (∼10-fold lower than those used clinically with collagen sponges in humans, after scaling by defect dimensions),[59] we observed robust new bone formation across nearly the entire defect site. Our earlier study showed that HA−PELA could effectively sensitize the response of MSCs to osteogenic induction by orders of magnitude compared to conventional degradable scaffolds in vitro.[7] We hypothesized that the bioactive HA−PELA spiral may also sensitize the response of the endogenous progenitor cells that migrated and adhered onto the scaffold to the osteogenic induction by the locally released rhBMP-2 in vivo. Indeed, the new bone formed with rhBMP-2 induction was not only significantly higher in volume than those templated by HA−PELA alone or HA−PELA + MSCs (Figure 7B) but also appeared more mature as revealed by polarized light microscopy (Figure 5B) and the

DOI: 10.1021/am508984y
ACS Appl. Mater. Interfaces 2015, 7, 4890−4901

substantial recanalization of new bone by 12 weeks (Figure 6). However, the new bone formed by rhBMP-2 induction appeared less templated by the spiral configuration than the bone formed in the MSC group. This may be due to the released rhBMP-2 being less confined to the immediate vicinity of the spiral template, resulting in greater bone formation both in between the spirally wrapped layers and on the scaffold outer periphery. By contrast, the possible direct participation of exogenous MSCs adhered to the HA−PELA could explain why new bone formation was exquisitely templated by the spiral-wrapped scaffold. However, the difficulty in tracking and colocalizing the exogenous MSCs by IHC within the newly formed bone over a longer period of time prevents us from obtaining more conclusive direct evidence.

It should be pointed out that the elastomeric nature of PELA results in a compressive modulus significantly lower than cortical (GPa scale) or trabecular bone (MPa scale), even for bulk rapid prototyped HA−PELA scaffolds (150 kPa compressive modulus).[69] Not as strong as other load-bearing synthetic bone grafting materials,[70] our HA−PELA scaffolds are insufficient for load-bearing applications without auxiliary load-bearing fixation (e.g., PEEK plate fixator used in this study). Also, the efficacy of spiral-wrapped HA−PELA scaffolds, with weight-bearing fixation, in augmenting the healing of critical-size long bone defects in large animals remains to be determined.

It should also be noted that restoration of the torsional strength of the defect was not achieved by 12 weeks in any of the treatment groups (Figure S4, Supporting Information). The 12 week time frame in the current study was not sufficient to examine whether the spiral-templated new bone growth in between adjacent scaffold layers would eventually merge into more mature and congruent bone as the scaffold fully degrades. Fusion of the concentrically distributed new bone layers could potentially be accelerated by introducing macropores in the spiral-wrapped electrospun scaffold, similar to the design proposed by Jiang et al.[37] Meanwhile, doubling the loading dose of rhBMP-2 from the exceptionally low 500 ng/defect applied in the current study, but still lower than the 2−11 μg per 5 mm segmental defect utilized with most literature scaffolds,[32,43,49,71−73] may also expedite the functional healing of the defect. Finally, applying a combination of exogenous cells, therapeutic agents, or both to the spiral-wrapped scaffold to synergistically stimulate the osteogenesis and angiogenesis may also present an opportunity to further improve the functional outcome of bone repair.

5. CONCLUSION

We tested whether the in vitro bioactivity of electrospun HA−PELA combined with its unique physical characteristics would translate spiral-wrapped electrospun HA−PELA scaffolds into a simple standalone scaffold for effective delivery of exogenous MSCs or rhBMP-2 and templated bone formation within critical-size long bone defects. The HA−PELA scaffold was readily seeded with MSCs or loaded with rhBMP-2, spiral-wrapped, and stably implanted into 5 mm midshaft femoral segmental defects in rats. The transplanted MSCs remained viable and well spread on the scaffold at least 1 week after implantation, whereas the preabsorbed rhBMP-2 was released from the scaffold in a sustained manner with retained bioactivity. We compared the bone repair templated by the scaffold seeded with exogenous MSCs to the repair enabled by endogenous cells recruited onto the scaffold with or without a low dose of rhBMP-2. We show that HA−PELA alone, preseeded with MSCs, or with a low dose of rhBMP-2 (500 ng) all supported varying degrees of bone formation within the defect. Bone formation was exquisitely templated by the spiral-wrapped scaffold when combined with MSCs, resulting in the formation of laminated new bone sandwiched in between adjacent electrospun scaffold layers. The most robust bone formation bridging over the scaffold-filled defect was obtained with the use of a single low dose of 500 ng rhBMP-2, although the distribution of the new bone within the scaffold did not precisely mirror the spiral-wrapped template. Overall, we demonstrated that spiral-wrapped electrospun HA−PELA scaffolds are both effective delivery vehicles for exogenous progenitor cells/protein therapeutics and viable standalone synthetic templates for guiding the repair of long bone defects. This work shows that the in vitro bioactivity of electrospun scaffolds can indeed translate to robust in vivo healing outcomes. The design and validation of such simple and scalable scaffolds is important for the clinical translation of tissue-engineered materials for bone repair.

■ ASSOCIATED CONTENT

Supporting Information

Optimization of lentiviral transduction of MSCs with GFP, high-magnification histology images, scavenger organ histology, and torsional testing of femurs. This material is available free of charge via the Internet at http://pubs.acs.org.

■ AUTHOR INFORMATION

Corresponding Author

*Phone: 508-334-7168. Fax: 508-334-2770. E-mail: Jie.Song@umassmed.edu.

Author Contributions

The manuscript was written through contributions of all authors. All authors have given approval to the final version of the manuscript.

Notes

The authors declare no competing financial interest.

■ ACKNOWLEDGMENTS

We thank April Mason-Savas for histology support and Dr. Ali Akalin for assessment of immune cell penetration. This research was supported in part by the National Institutes of Health Grant R01AR055615 and by the Department of Defense Congressionally Directed Medical Research Programs under award number W81XWH-10-0574. Core resources supported by the National Institutes of Health shared instrumentation grant S10RR027082 were used.

■ REFERENCES

(1) Faour, O.; Dimitriou, R.; Cousins, C. A.; Giannoudis, P. V. The Use of Bone Graft Substitutes in Large Cancellous Voids: Any Specific Needs? *Injury* **2011**, *42* (Suppl 2), S87−S90.

(2) Wheeler, D. L.; Enneking, W. F. Allograft Bone Decreases in Strength In Vivo over Time. *Clin. Orthop. Relat. Res.* **2005**, 36−42.

(3) Place, E. S.; Evans, N. D.; Stevens, M. M. Complexity in Biomaterials for Tissue Engineering. *Nat. Mater.* **2009**, *8*, 457−470.

(4) Li, W. J.; Laurencin, C. T.; Caterson, E. J.; Tuan, R. S.; Ko, F. K. Electrospun Nanofibrous Structure: A Novel Scaffold for Tissue Engineering. *J. Biomed. Mater. Res.* **2002**, *60*, 613−621.

(5) Lyu, S.; Huang, C.; Yang, H.; Zhang, X. Electrospun Fibers as a Scaffolding Platform for Bone Tissue Repair. *J. Orthop. Res.* **2013**, *31*, 1382−1389.

DOI: 10.1021/am508984y
ACS Appl. Mater. Interfaces 2015, 7, 4890−4901

(6) Li, W. J.; Tuli, R.; Huang, X.; Laquerriere, P.; Tuan, R. S. Multilineage Differentiation of Human Mesenchymal Stem Cells in a Three-Dimensional Nanofibrous Scaffold. *Biomaterials* **2005**, *26*, 5158−5166.
(7) Kutikov, A. B.; Song, J. An Amphiphilic Degradable Polymer/hydroxyapatite Composite with Enhanced Handling Characteristics Promotes Osteogenic Gene Expression in Bone Marrow Stromal Cells. *Acta Biomater.* **2013**, *9*, 8354−8364.
(8) Filion, T. M.; Kutikov, A.; Song, J. Chemically Modified Cellulose Fibrous Meshes for Use as Tissue Engineering Scaffolds. *Bioorg. Med. Chem. Lett.* **2011**, *21*, 5067−5070.
(9) Ngiam, M.; Liao, S.; Patil, A. J.; Cheng, Z.; Chan, C. K.; Ramakrishna, S. The Fabrication of Nano-Hydroxyapatite on PLGA and PLGA/collagen Nanofibrous Composite Scaffolds and Their Effects in Osteoblastic Behavior for Bone Tissue Engineering. *Bone* **2009**, *45*, 4−16.
(10) Phipps, M. C.; Clem, W. C.; Catledge, S. A.; Xu, Y.; Hennessy, K. M.; Thomas, V.; Jablonsky, M. J.; Chowdhury, S.; Stanishevsky, A. V.; Vohra, Y. K.; Bellis, S. L. Mesenchymal Stem Cell Responses to Bone-Mimetic Electrospun Matrices Composed of Polycaprolactone, Collagen I and Nanoparticulate Hydroxyapatite. *PLoS One* **2011**, *6*, e16813.
(11) D'Angelo, F.; Armentano, I.; Cacciotti, I.; Tiribuzi, R.; Quattrocelli, M.; Del Gaudio, C.; Fortunati, E.; Saino, E.; Caraffa, A.; Cerulli, G. G.; Visai, L.; Kenny, J. M.; Sampaolesi, M.; Bianco, A.; Martino, S.; Orlacchio, A. Tuning Multi/pluri-Potent Stem Cell Fate by Electrospun poly(L-Lactic Acid)-Calcium-Deficient Hydroxyapatite Nanocomposite Mats. *Biomacromolecules* **2012**, *13*, 1350−1360.
(12) Supová, M. Problem of Hydroxyapatite Dispersion in Polymer Matrices: A Review. *J. Mater. Sci. Mater. Med.* **2009**, *20*, 1201−1213.
(13) Wagoner Johnson, A. J.; Herschler, B. A. A Review of the Mechanical Behavior of CaP and CaP/polymer Composites for Applications in Bone Replacement and Repair. *Acta Biomater.* **2011**, *7*, 16−30.
(14) Wang, M. Developing Bioactive Composite Materials for Tissue Replacement. *Biomaterials* **2003**, *24*, 2133−2151.
(15) Venugopal, J.; Low, S.; Choon, A. T.; Bharath Kumar, A.; Ramakrishna, S. Electrospun-Modified Nanofibrous Scaffolds for the Mineralization of Osteoblast Cells. *J. Biomed. Mater. Res., Part A* **2008**, *85*, 408−417.
(16) Dinarvand, P.; Seyedjafari, E.; Shafiee, A.; Babaei Jandaghi, A.; Doostmohammadi, A.; Fathi, M. H.; Farhadian, S.; Soleimani, M. New Approach to Bone Tissue Engineering: Simultaneous Application of Hydroxyapatite and Bioactive Glass Coated on a poly(L-Lactic Acid) Scaffold. *ACS Appl. Mater. Interfaces* **2011**, *3*, 4518−4524.
(17) Rasal, R. M.; Janorkar, A. V.; Hirt, D. E. Poly(lactic Acid) Modifications. *Prog. Polym. Sci.* **2010**, *35*, 338−356.
(18) Kim, H.; Lee, H.; Knowles, J. C. Electrospinning Biomedical Nanocomposite Fibers of Hydroxyapatite/poly(lactic Acid) for Bone Regeneration. *J. Biomed. Mater. Res., Part A* **2006**, *79*, 643−649.
(19) Dupraz, A. M. P.; de Wijn, J. R.; v. d. Meer, S. A. T.; de Groot, K. Characterization of Silane-Treated Hydroxyapatite Powders for Use as Filler in Biodegradable Composites. *J. Biomed. Mater. Res.* **1996**, *30*, 231−238.
(20) Dupraz, A. M. P.; v. d. Meer, S. A. T.; De Wijn, J. R.; Goedemoed, J. H. Biocompatibility Screening of Silane-Treated Hydroxyapatite Powders, for Use as Filler in Resorbable Composites. *J. Mater. Sci. Mater. Med.* **1996**, *7*, 731−738.
(21) Zhang, P.; Hong, Z.; Yu, T.; Chen, X.; Jing, X. In Vivo Mineralization and Osteogenesis of Nanocomposite Scaffold of Poly(lactide-Co-Glycolide) and Hydroxyapatite Surface-Grafted with Poly(l-Lactide). *Biomaterials* **2009**, *30*, 58−70.
(22) Yamaoka, T.; Tabata, Y.; Ikada, Y. Distribution and Tissue Uptake of Poly(ethylene Glycol) with Different Molecular Weights after Intravenous Administration to Mice. *J. Pharm. Sci.* **1994**, *83*, 601−606.
(23) Hwang, N. S.; Varghese, S.; Lee, H. J.; Zhang, Z.; Elisseeff, J. Biomaterials Directed In Vivo Osteogenic Differentiation of Mesenchymal Cells Derived from Human Embryonic Stem Cells. *Tissue Eng., Part A* **2013**, *19*, 1723−1732.
(24) Göpferich, A.; Peter, S. J.; Lucke, A.; Lu, L.; Mikos, A. G. Modulation of Marrow Stromal Cell Function Using poly(D,L-Lactic Acid)-Block-Poly(ethylene Glycol)-Monomethyl Ether Surfaces. *J. Biomed. Mater. Res.* **1999**, *46*, 390−398.
(25) Lieb, E.; Tessmar, J.; Hacker, M.; Fischbach, C.; Rose, D.; Blunk, T.; Mikos, A. G.; Göpferich, A.; Schulz, M. B. Poly (D, L-Lactic Acid)-Poly (ethylene Glycol)-Monomethyl Ether Diblock Copolymers Control Adhesion and Osteoblastic Differentiation of Marrow Stromal Cells. *Tissue Eng.* **2003**, *9*, 71−84.
(26) Altankov, G.; Thom, V.; Groth, T.; Jankova, K.; Jonsson, G.; Ulbricht, M. Modulating the Biocompatibility of Polymer Surfaces with Poly(ethylene Glycol): Effect of Fibronectin. *J. Biomed. Mater. Res.* **2000**, *52*, 219−230.
(27) Horner, E. A.; Kirkham, J.; Wood, D.; Curran, S.; Smith, M.; Thomson, B.; Yang, X. B. Long Bone Defect Models for Tissue Engineering Applications: Criteria for Choice. *Tissue Eng., Part B* **2010**, *16*, 263−271.
(28) Song, J.; Xu, J.; Filion, T.; Saiz, E.; Tomsia, A. P.; Lian, J. B.; Stein, G. S.; Ayers, D. C.; Bertozzi, C. R. Elastomeric High-Mineral Content Hydrogel-Hydroxyapatite Composites for Orthopedic Applications. *J. Biomed. Mater. Res., Part A* **2009**, *89*, 1098−1107.
(29) Miao, D.; Scutt, A. Histochemical Localization of Alkaline Phosphatase Activity in Decalcified Bone and Cartilage. *J. Histochem. Cytochem.* **2002**, *50*, 333−340.
(30) Filion, T. M.; Li, X.; Mason-Savas, A.; Kreider, J. M.; Goldstein, S. A.; Ayers, D. C.; Song, J. Elastomeric Osteoconductive Synthetic Scaffolds with Acquired Osteoinductivity Expedite the Repair of Critical Femoral Defects in Rats. *Tissue Eng., Part A* **2011**, *17*, 503−511.
(31) Hsu, W. K.; Sugiyama, O.; Park, S. H.; Conduah, A.; Feeley, B. T.; Liu, N. Q.; Krenek, L.; Virk, M. S.; An, D. S.; Chen, I. S.; Lieberman, J. R. Lentiviral-Mediated BMP-2 Gene Transfer Enhances Healing of Segmental Femoral Defects in Rats. *Bone* **2007**, *40*, 931−938.
(32) Brown, K. V.; Li, B.; Guda, T.; Perrien, D. S.; Guelcher, S. A.; Wenke, J. C. Improving Bone Formation in a Rat Femur Segmental Defect by Controlling Bone Morphogenetic Protein-2 Release. *Tissue Eng., Part A* **2011**, *17*, 1735−1746.
(33) Rai, B.; Oest, M. E.; Dupont, K. M.; Ho, K. H.; Teoh, S. H.; Guldberg, R. E. Combination of Platelet-Rich Plasma with Polycaprolactone-Tricalcium Phosphate Scaffolds for Segmental Bone Defect Repair. *J. Biomed. Mater. Res., Part A* **2007**, *81*, 888−899.
(34) Rodriguez-Merchan, E. C.; Forriol, F. Nonunion: General Principles and Experimental Data. *Clin. Orthop. Relat. Res.* **2004**, 4−12.
(35) Sato, K.; Watanabe, Y.; Harada, N.; Abe, S.; Matsushita, T.; Yamanaka, K.; Kaneko, T.; Sakai, Y. Establishment of Reproducible, Critical-Sized, Femoral Segmental Bone Defects in Rats. *Tissue Eng., Part C* **2014**, 1−5.
(36) Williams, D. F. On the Mechanisms of Biocompatibility. *Biomaterials* **2008**, *29*, 2941−2953.
(37) Jiang, H.; Zuo, Y.; Zou, Q.; Wang, H.; Du, J.; Li, Y.; Yang, X. Biomimetic Spiral-Cylindrical Scaffold Based on Hybrid Chitosan/cellulose/nano-Hydroxyapatite Membrane for Bone Regeneration. *ACS Appl. Mater. Interfaces* **2013**, *5*, 12036−12044.
(38) Pişkin, E.; Işoğlu, I. A.; Bölgen, N.; Vargel, I.; Griffiths, S.; Cavuşoğlu, T.; Korkusuz, P.; Güzel, E.; Cartmell, S. In Vivo Performance of Simvastatin-Loaded Electrospun Spiral-Wound Polycaprolactone Scaffolds in Reconstruction of Cranial Bone Defects in the Rat Model. *J. Biomed. Mater. Res., Part A* **2009**, *90*, 1137−1151.
(39) Wang, J.; Valmikinathan, C. M.; Liu, W.; Laurencin, C. T.; Yu, X. Spiral-Structured, Nanofibrous, 3D Scaffolds for Bone Tissue Engineering. *J. Biomed. Mater. Res., Part A* **2010**, *93*, 753−762.
(40) Zhang, X.; Chang, W.; Lee, P.; Wang, Y.; Yang, M.; Li, J.; Kumbar, S. G.; Yu, X. Polymer-Ceramic Spiral Structured Scaffolds for Bone Tissue Engineering: Effect of Hydroxyapatite Composition on Human Fetal Osteoblasts. *PLoS One* **2014**, *9*, e85871.

DOI: 10.1021/am508984y
ACS Appl. Mater. Interfaces 2015, 7, 4890−4901

(41) Wang, J.; Yu, X. Preparation, Characterization and in Vitro Analysis of Novel Structured Nanofibrous Scaffolds for Bone Tissue Engineering. *Acta Biomater.* **2010**, *6*, 3004−3012.
(42) Kolambkar, Y. M.; Dupont, K. M.; Boerckel, J. D.; Huebsch, N.; Mooney, D. J.; Hutmacher, D. W.; Guldberg, R. E. An Alginate-Based Hybrid System for Growth Factor Delivery in the Functional Repair of Large Bone Defects. *Biomaterials* **2011**, *32*, 65−74.
(43) Kolambkar, Y. M.; Boerckel, J. D.; Dupont, K. M.; Bajin, M.; Huebsch, N.; Mooney, D. J.; Hutmacher, D. W.; Guldberg, R. E. Spatiotemporal Delivery of Bone Morphogenetic Protein Enhances Functional Repair of Segmental Bone Defects. *Bone* **2011**, *49*, 485−492.
(44) Berner, a; Boerckel, J. D.; Saifzadeh, S.; Steck, R.; Ren, J.; Vaquette, C.; Zhang, J. Q.; Nerlich, M.; Guldberg, R. E.; Hutmacher, D. W.; Woodruff, M. A. Biomimetic Tubular Nanofiber Mesh and Platelet Rich Plasma-Mediated Delivery of BMP-7 for Large Bone Defect Regeneration. *Cell Tissue Res.* **2012**, *347*, 603−612.
(45) Shin, M.; Yoshimoto, H.; Vacanti, J. P. In Vivo Bone Tissue Engineering Using Mesenchymal Stem Cells on a Novel Electrospun Nanofibrous Scaffold. *Tissue Eng.* **2004**, *10*, 33−41.
(46) Fu, S.; Ni, P.; Wang, B.; Chu, B.; Peng, J.; Zheng, L.; Zhao, X.; Luo, F.; Wei, Y.; Qian, Z. In Vivo Biocompatibility and Osteogenesis of Electrospun Poly(ε-Caprolactone)-Poly(ethylene Glycol)-Poly(ε-Caprolactone)/nano-Hydroxyapatite Composite Scaffold. *Biomaterials* **2012**, *33*, 8363−8371.
(47) Ko, E. K.; Jeong, S. I.; Rim, N. G.; Lee, Y. M.; Shin, H.; Lee, B. K. In Vitro Osteogenic Differentiation of Human Mesenchymal Stem Cells and in Vivo Bone Formation in Composite Nanofiber Meshes. *Tissue Eng., Part A* **2008**, *14*, 2105−2119.
(48) Woo, K. M.; Chen, V. J.; Jung, H.-M.; Kim, T. I.; Shin, H. I.; Baek, J. H.; Ryoo, H. M.; Ma, P. X. Comparative Evaluation of Nanofibrous Scaffolding for Bone Regeneration in Critical-Size Calvarial Defects. *Tissue Eng., Part A* **2009**, *15*, 2155−2162.
(49) Yasko, A. W.; Lane, J. M.; Fellinger, E. J.; Rosen, V.; Wozney, J. M.; Wang, E. A. The Healing of Segmental Bone Defects, Induced by Recombinant Human Bone Morphogenetic Protein (rhBMP-2). A Radiographic, Histological, and Biomechanical Study in Rats. *J. Bone Joint Surg. Am.* **1992**, *74*, 659−670.
(50) Dupont, K. M.; Sharma, K.; Stevens, H. Y.; Boerckel, J. D.; García, A. J.; Guldberg, R. E. Human Stem Cell Delivery for Treatment of Large Segmental Bone Defects. *Proc. Natl. Acad. Sci. U.S.A.* **2010**, *107*, 3305−3310.
(51) Kadiyala, S.; Jaiswal, N.; Bruder, S. S. P. Culture-Expanded, Bone Marrow-Derived Mesenchymal Stem Cells Can Regenerate a Critical-Sized Segmental Bone Defect. *Tissue Eng.* **1997**, *3*, 173−185.
(52) Schantz, J. T.; Hutmacher, D. W.; Lam, C. X. F.; Brinkmann, M.; Wong, K. M.; Lim, T. C.; Chou, N.; Guldberg, R. E.; Teoh, S. H. Repair of Calvarial Defects with Customised Tissue-Engineered Bone Grafts II. Evaluation of Cellular Efficiency and Efficacy in Vivo. *Tissue Eng.* **2003**, *9* (Suppl1), S127−S139.
(53) Tasso, R.; Augello, A.; Boccardo, S.; Salvi, S.; Caridà, M.; Postiglione, F.; Fais, F.; Truini, M.; Cancedda, R.; Pennesi, G. Recruitment of a Host's Osteoprogenitor Cells Using Exogenous Mesenchymal Stem Cells Seeded on Porous Ceramic. *Tissue Eng., Part A* **2009**, *15*, 2203−2212.
(54) Tasso, R.; Gaetani, M.; Molino, E.; Cattaneo, A.; Monticone, M.; Bachi, A.; Cancedda, R. The Role of bFGF on the Ability of MSC to Activate Endogenous Regenerative Mechanisms in an Ectopic Bone Formation Model. *Biomaterials* **2012**, *33*, 2086−2096.
(55) Crisostomo, P. R.; Markel, T. a; Wang, Y.; Meldrum, D. R. Surgically Relevant Aspects of Stem Cell Paracrine Effects. *Surgery* **2008**, *143*, 577−581.
(56) Zimmermann, C. E.; Gierloff, M.; Hedderich, J.; Açil, Y.; Wiltfang, J.; Terheyden, H. Survival of Transplanted Rat Bone Marrow-Derived Osteogenic Stem Cells in Vivo. *Tissue Eng., Part A* **2011**, *17*, 1147−1156.
(57) Hwang, S. J.; Cho, T. H.; Kim, I. S. In Vivo Gene Activity of Human Mesenchymal Stem Cells After Scaffold-Mediated Local Transplantation. *Tissue Eng., Part A* **2014**, 1−15.
(58) McKay, W. F.; Peckham, S. M.; Badura, J. M. A Comprehensive Clinical Review of Recombinant Human Bone Morphogenetic Protein-2 (INFUSE Bone Graft). *Int. Orthop.* **2007**, *31*, 729−734.
(59) Suzuki, S.; Ikada, Y. *Biomaterials for Surgical Operation*; Springer: New York, 2011; p 200.
(60) Sibiya, S. J.; Olivier, E. I.; Duneas, N. High Yield Isolation of BMP-2 from Bone and in Vivo Activity of a Combination of BMP-2/TGF-β1. *J. Biomed. Mater. Res., Part A* **2013**, *101*, 641−646.
(61) Epstein, N. E. Pros, Cons, and Costs of INFUSE in Spinal Surgery. *Surg. Neurol. Int.* **2011**, *2*, 10.
(62) Epstein, N. E. Complications due to the Use of BMP/INFUSE in Spine Surgery: The Evidence Continues to Mount. *Surg. Neurol. Int.* **2013**, *4*, S343−S352.
(63) Cho, T.-J.; Gerstenfeld, L. C.; Einhorn, T. A. Differential Temporal Expression of Members of the Transforming Growth Factor Beta Superfamily during Murine Fracture Healing. *J. Bone Miner. Res.* **2002**, *17*, 513−520.
(64) Katagiri, T.; Yamaguchi, A.; Komaki, M.; Abe, E.; Takahashi, N.; Ikeda, T.; Rosen, V.; Wozney, J. M.; Fujisawa-Sehara, A.; Suda, T. Bone Morphogenetic Protein-2 Converts the Differentiation Pathway of C2C12 Myoblasts into the Osteoblast Lineage. *J. Cell Biol.* **1994**, *127*, 1755−1766.
(65) Filion, T. M.; Xu, J.; Prasad, M. L.; Song, J. In Vivo Tissue Responses to Thermal-Responsive Shape Memory Polymer Nanocomposites. *Biomaterials* **2011**, *32*, 985−991.
(66) Suganuma, J.; Alexander, H. Biological Response of Intramedullary Bone to Poly-L-Lactic Acid. *J. Appl. Biomater.* **1993**, *4*, 13−27.
(67) Agrawal, C. M.; Athanasiou, K. A. Technique to Control pH in Vicinity of Biodegrading PLA-PGA Implants. *J. Biomed. Mater. Res.* **1997**, *38*, 105−114.
(68) Zhong, S.; Zhang, Y.; Lim, C. T. Fabrication of Large Pores in Electrospun Nanofibrous Scaffolds for Cellular Infiltration: A Review. *Tissue Eng., Part B* **2012**, *18*, 77−87.
(69) Kutikov, A. B.; Gurijala, A.; Song, J. Rapid Prototyping Amphiphilic Polymer/Hydroxyapatite Composite Scaffolds with Hydration-Induced Self-Fixation Behavior. *Tissue Eng., Part C* **2014**, DOI: 10.1089/ten.TEC.2014.0213.
(70) Xu, N.; Ye, X.; Wei, D.; Zhong, J.; Chen, Y.; Xu, G.; He, D. 3D Artificial Bones for Bone Repair Prepared by Computed Tomography-Guided Fused Deposition Modeling for Bone Repair. *ACS Appl. Mater. Interfaces* **2014**, *6*, 14952−14963.
(71) Zara, J. N.; Siu, R. K.; Zhang, X.; Shen, J.; Ngo, R.; Lee, M.; Li, W.; Chiang, M.; Chung, J.; Kwak, J.; Wu, M. B.; Ting, K.; Soo, C. High Doses of Bone Morphogenetic Protein 2 Induce Structurally Abnormal Bone and Inflammation In Vivo. *Tissue Eng., Part A* **2011**, *17*, 1389−1399.
(72) Kirker-Head, C.; Karageorgiou, V.; Hofmann, S.; Fajardo, R.; Betz, O.; Merkle, H. P.; Hilbe, M.; von Rechenberg, B.; McCool, J.; Abrahamsen, L.; Nazarian, A.; Cory, E.; Curtis, M.; Kaplan, D.; Meinel, L. BMP-Silk Composite Matrices Heal Critically Sized Femoral Defects. *Bone* **2007**, *41*, 247−255.
(73) Lee, S. S.; Huang, B. J.; Kaltz, S. R.; Sur, S.; Newcomb, C. J.; Stock, S. R.; Shah, R. N.; Stupp, S. I. Bone Regeneration with Low Dose BMP-2 Amplified by Biomimetic Supramolecular Nanofibers within Collagen Scaffolds. *Biomaterials* **2013**, *34*, 452−459.

DOI: 10.1021/am508984y
ACS Appl. Mater. Interfaces 2015, 7, 4890−4901